that we are unable to explain satisfactorily. The simplest interpretation of the results is that the Arrhenius plot shown in Figure 3 is linear. While this approach yields reasonable Arrhenius parameters and makes sense theoretically, it does not seem wholly consistent with the data. Conversely, a two reaction channel model can give good agreement with experiment but yields an extraordinarily high A factor for the T-dependent channel. Although we could not measure the rate coefficient for reaction 1 at the temperatures prevalent in the upper atmosphere of Titan (150–170 K), the temperature dependence of the reaction suggests that the rate constant for the N + CH_3 reaction will not be substantially lower than the value at 200 K. Therefore, it seems likely that the reaction is an important C–N bond-forming process in Titan's atmosphere.

It is important that the experiments described in this work are repeated, preferably with a different technique and over an extended temperature range. Theoretical investigations and a study of the branching ratio of the reaction are also important. Experiments on the product distribution of reaction 1 as a function of temperature are in progress in our laboratory.

Acknowledgment. This work was supported by the NASA Planetary Atmospheres Program. F.L.N. acknowledges support under NASA Grant NSG-5173 to The Catholic University of America. G.M. thanks the National Research Council/National Academy of Sciences for the award of a Research Associateship.

Registry No. N, 17778-88-0; CH_3, 2229-07-4; N_2, 7727-37-9; CH_4, 74-82-8; F, 14762-94-8; HCN, 74-90-8.

Intrinsic Frequency Analysis of the Generalized Normal-Mode Vibrations for the Reaction $H_2 + CH_3 \rightarrow H + CH_4$

Jerry A. Boatz and Mark S. Gordon*

Department of Chemistry, North Dakota State University, Fargo, North Dakota 58105
(Received: November 28, 1988; In Final Form: February 20, 1989)

Vibrational energy distributions and intrinsic frequencies are computed at selected points along the $H_2 + CH_3 \rightarrow H + CH_4$ intrinsic reaction coordinate, calculated at the UHF/STO-3G level. The energy distributions and intrinsic frequencies are shown to provide a clear and intuitively pleasing picture of the evolution of generalized normal coordinates along the reaction path. Furthermore, these quantities aid in the identification of avoided crossings between distinct generalized normal modes and between generalized normal modes and the reaction coordinate.

I. Introduction

A common problem in the field of reaction path dynamics is the determination of vibrational modes and frequencies of a molecular complex along a reaction path.[1-3] In particular, the interactions of the individual modes with each other and with the reaction path itself must be characterized in order to obtain the curvature[1,3-5] of the path, which in turn is required to calculate tunneling effects.[3-5] The usual procedure[3,5] is to compute derivatives of the generalized normal-coordinate vectors with respect to the reaction path coordinate. While such calculations are necessary for the quantitative determination of reaction path curvature, they indicate only that an interaction takes place; the details of the nature of the interaction itself are not revealed.

The vibrational energy distribution scheme of Pulay and coworkers[6] and the intrinsic frequency method of J.A.B. and M.S.G.[7] are convenient methods for the description of normal modes in terms of internal coordinates. However, until now, these schemes have only been applied to molecules at their equilibrium geometries.[6,7] As will be demonstrated below, the calculation of the vibrational energy distributions and intrinsic frequencies along a reaction path provides a vivid picture of the evolution of generalized normal modes during the course of a chemical reaction.

II. Computational Method

The $H_2 + CH_3 \rightarrow H + CH_4$ abstraction reaction was chosen to illustrate the application of vibrational energy distributions[6] and intrinsic frequencies[7] to the analysis of a reaction coordinate. While moderate in size, this reaction exhibits a number of interesting features. For instance, on the products side of the reaction, a bifurcation[8] occurs on the intrinsic reaction coordinate (IRC)[9,10] at the UHF/STO-3G[11] computational level. At a higher level of calculation (i.e., using a larger basis set and/or including correlation corrections), the details of this reaction coordinate may differ. We have chosen to use a minimal basis set simply for the purpose of illustration and not as an accurate representation of the CH_5 potential energy surface. The transition-state structure was located and verified with a modified version of GAUSSIAN86.[12] The IRC was generated with GAMESS[13] with the stabilized Euler method[5,10,13] and a step size of 0.05 bohr·amu$^{1/2}$. (For a more

(1) Miller, W. H.; Handy, N. C.; Adams, J. E. *J. Chem. Phys.* **1980**, *72*, 99–112.
(2) Yamashita, K.; Yamabe, T. *Int. J. Quantum Chem., Quantum Chem. Symp.* **1983**, *17*, 177–189.
(3) Truhlar, D. G.; Isaacson, A. D.; Garrett, B. C. In *Theory of Chemical Reaction Dynamics*; Baer, M., Ed.; CRC: Boca Raton, FL, 1985.
(4) Page, M.; McIver, J. W., Jr. *J. Chem. Phys.* **1988**, *88*, 922–935.
(5) (a) Baldridge, K. K. Ph.D. Thesis, North Dakota State University, Fargo, ND, 1988, and references therein. (b) Baldridge, K. K.; Gordon, M. S.; Steckler, R.; Truhlar, D. G. *J. Phys. Chem.*, submitted for publication.
(6) (a) Pulay, P.; Török, F. *Acta Chim. Acad. Sci. Hung.* **1966**, *47*, 273–279. (b) Morino, Y.; Kuchitsu, K. *J. Chem. Phys.* **1952**, *20*, 1809–1810. (c) See, for example: Keresztury, G.; Jalsovszky, Gy. *J. Mol. Struct.* **1971**, *10*, 304–305.
(7) Boatz, J. A.; Gordon, M. S. *J. Phys. Chem.* **1989**, *93*, 1819–1826.
(8) Valtazanos, P.; Ruedenberg, K. *Theor. Chim. Acta* **1986**, *69*, 281–307.
(9) (a) Fukui, K. *Acc. Chem. Res.* **1981** *14*, 363–368. (b) Fukui, K. *Pure Appl. Chem.* **1982**, *54*, 1825–1836. (c) Fukui, K. *Int. J. Quantum Chem., Quantum Chem. Symp.* **1981**, *15*, 633–642.
(10) (a) Ishida, K.; Morokuma, K.; Komornicki, A. *J. Chem. Phys.* **1977**, *66*, 2153–2156. (b) Schmidt, M. W.; Gordon, M. S.; Dupuis, M. *J. Am. Chem. Soc.* **1985**, *107*, 2585–2589.
(11) (a) Hehre, W. J.; Stewart, R. F.; Pople, J. A. *J. Chem. Phys.* **1969**, *51*, 2657–2664. (b) Hehre, W. J.; Ditchfield, R.; Stewart, R. F.; Pople, J. A. *J. Chem. Phys.* **1970**, *52*, 2769–2773.
(12) Frisch, M. J.; Binkley, J. S.; Schlegel, H. B.; Raghavachari, K.; Melius, C. F.; Martin, R. L.; Stewart, J. J. P.; Bobrowicz, F. W.; Rohling, C. M.; Kahn, L. R.; Defrees, D. J.; Seeger, R.; Whiteside, R. A.; Fox, D. J.; Fleuder, E. M.; Pople, J. A. *GAUSSIAN86*; Carnegie-Mellon Quantum Chemistry Publishing Unit: Pittsburgh, PA, 1984.

0022-3654/89/2093-5774$01.50/0

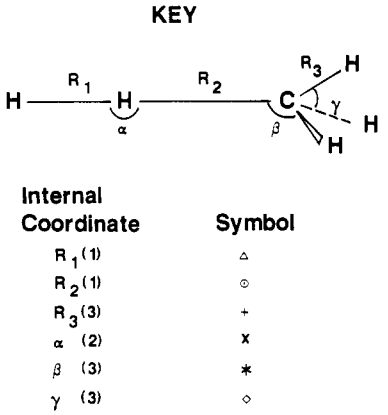

Figure 1. Symbol scheme used in Figures 3, 5, and 6. The number of symmetrically equivalent coordinates for each internal parameter is given in parentheses.

complete analysis of this reaction, see ref 5.) The Cartesian force constant matrix was computed at 10 (approximately equally spaced) points on both the reactants and products side of the reaction. The reaction coordinate was then removed from the force constant matrices by the projection scheme of Miller, Handy, and Adams.[1] The eigenvalues and eigenvectors obtained from this projection procedure will be referred to as "generalized normal modes".

The computation of energy distributions and intrinsic frequencies is summarized as follows:[7] The Cartesian force constant matrix **f** is defined by

$$\mathbf{f}_{ij} = \partial^2 E / \partial x_i \partial x_j \tag{1}$$

where E is the internal molecular energy and x_i, x_j are Cartesian nuclear coordinates. Similarly, the internal coordinate force constant matrix **F** is defined by

$$\mathbf{F}_{ij} = \partial^2 E / \partial r_i \partial r_j \tag{2}$$

where r_i, r_j denote internal coordinates. The matrix **B** relates the Cartesian coordinate vector $\vec{X}$ to the vector of internal coordinates $\vec{R}$ by

$$\vec{R} = \mathbf{B}\vec{X} \tag{3}$$

If **l** is the matrix that diagonalizes **f**, then

$$\begin{aligned} \mathbf{\Lambda} &= \mathbf{l}^t\mathbf{f}\mathbf{l} \\ &= \mathbf{D}^t\mathbf{F}\mathbf{D} \end{aligned} \tag{4}$$

where $\mathbf{\Lambda}$ is the (diagonal) eigenvalue matrix and $\mathbf{D} = \mathbf{B}\mathbf{l}$. Equation 4 in scalar form is

$$\lambda_i = \sum_m \sum_n D_{mi} F_{mn} D_{ni} \tag{4'}$$

where $\lambda_i = \Lambda_{ii}$ is the ith eigenvalue of **f**. We define the vibrational density matrix $\mathbf{P}^i$ as

$$\mathbf{P}^i_{mn} = D_{mi} F_{mn} D_{ni} / \lambda_i \tag{5}$$

The energy distribution matrix **M** is obtained from $\mathbf{P}^i$ by

$$\mathbf{M}_{im} = \sum_n \mathbf{P}^i_{mn} \tag{6}$$

$\mathbf{M}_{im}$ can be interpreted[6a] as the fractional contribution of internal coordinate r_m to the ith generalized normal coordinate.

Finally, we define the intrinsic frequency ν_n[7] as

$$\nu_n = \sum_m \sum_i \mathbf{P}^i_{mn} \lambda_i \tag{7}$$

Each ν_n represents the total contribution of internal coordinate r_n to the normal-coordinate frequencies; i.e., ν_n is the frequency associated with the motion of a single internal coordinate r_n.

(13) Dupuis, M.; Spangler, D.; Wendoloski, J. J. NRCC Software Catalog, 1980, 1, Program QG01. Schmidt, M. W.; Boatz, J. A.; Baldridge, K. K.; Koseki, S.; Gordon, M. S.; Elbert, S. T.; Lam, B. *QCPE Bull.* **1987**, *7*, 115.

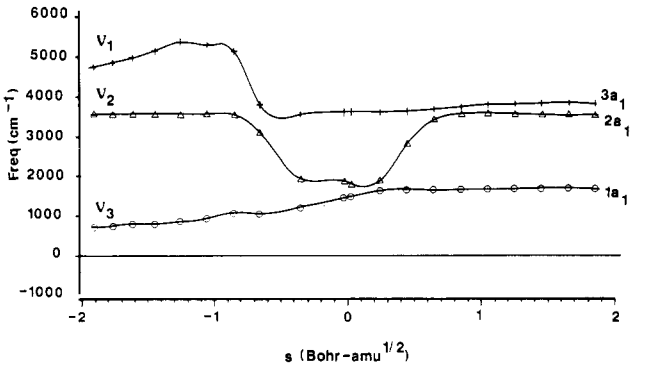

Figure 2. Generalized a_1 normal-coordinate frequencies (cm^{-1}) along the $H_2 + CH_3 \rightarrow H + CH_4$ IRC. The ν_n labels on the left side correspond to the labeling scheme used in ref 5.

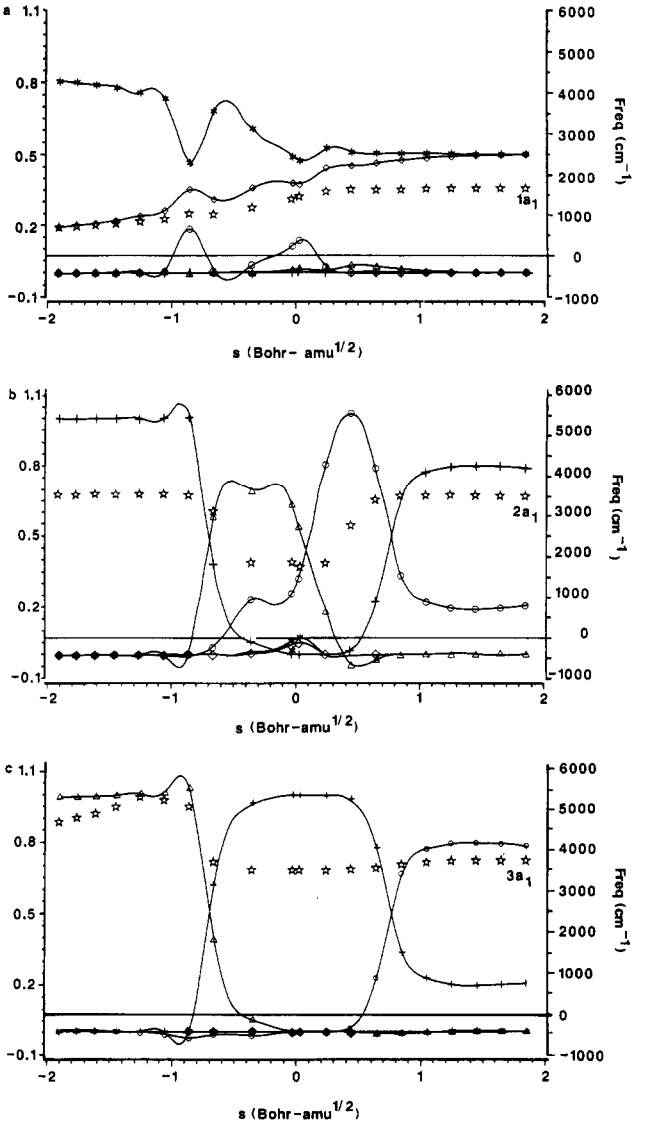

Figure 3. Vibrational energy distributions (smooth curves) of the generalized a_1 normal modes and their associated frequencies (☆; cm^{-1}). The vertical axis on the left is unitless.

III. Results and Discussion

Figure 1 outlines the symbol scheme used in Figures 3, 5, and 6. (The different plotting symbols in Figures 2 and 4 are for readability purposes only and do not correspond to the assignments indicated in Figure 1.) R_1 (△) is the breaking H–H bond, R_2 (⊙) is the forming C–H bond, and R_3 (+) represents the three equivalent C–H bonds that remain intact during the entire reaction (hereafter referred to as the intact C–H stretches). α (×) represents the two degenerate H–H–C linear bends and β (*) denotes

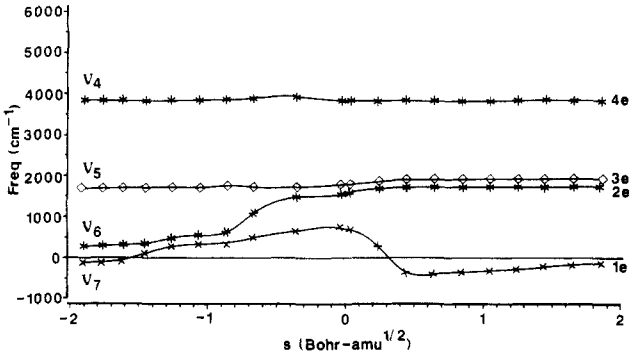

Figure 4. Generalized e normal-coordinate frequencies (cm^{-1}) along the $H_2 + CH_3 \rightarrow H + CH_4$ IRC. The ν_n labels on the left side correspond to the labeling scheme used in ref 5.

the three equivalent forming H–C–H bends. γ (◇) represents the three equivalent H–C–H bends that remain essentially unchanged throughout the reaction (hereafter referred to as the intact H–C–H bends). Finally, ☆ (not connected by smooth curves) in Figures 3 and 5 represent the associated projected normal-coordinate frequencies found in Figures 2 and 4. In Figures 3 and 5, the curves correspond to the vertical axis on the left, while the discrete points ☆ correspond to the vertical axis on the right. Note that, at the products ($H + CH_4$) end point of the reaction, R_2 and β become equivalent with R_3 and γ, respectively, and α is undefined. Likewise, at the reactants ($H_2 + CH_3$) end point, $R_2 \rightarrow \infty$ and so α and β become undefined.

A reaction channel of C_{3v} symmetry was assumed, and so the generalized normal-coordinate frequencies are designated in terms of a_1 and e irreducible representations. The reactants $H_2 + CH_3$ have six translations, five rotations, and seven vibrational degrees of freedom ($3a_1 \oplus 2e$). Along the reaction path, there are three translations, three rotations, and eleven vibrations ($3a_1 \oplus 4e$). The remaining degree of freedom, the a_1 "vibration" representing the reaction path trajectory, is removed in the projection[1] of the Hessians. Finally, the products $H + CH_4$ possess six translations, three rotations, and nine vibrations ($3a_1 \oplus 3e$).[2,5]

In Figures 2–6, the abscissa is the reaction path distance, with the negative values of s (left side) corresponding to reactants ($H_2 + CH_3$). Figure 2 is a plot of the harmonic frequencies of the a_1 generalized normal modes along the IRC. There are apparently three regions of possible avoided crossings between the a_1 modes. The first occurs around $s = -0.7$ and involves the $2a_1$ and $3a_1$ vibrations. The second occurs in the neighborhood of the transition state and presumably involves the $1a_1$ and $2a_1$ vibrations. The third occurs around $s = 0.7$ and again appears to involve $2a_1$ and $3a_1$. It should be kept in mind that the a_1 mode representing the reaction path does not appear since it has been projected out.

Parts a–c of Figure 3 depict the decompositions of the a_1 generalized normal modes in terms of the 13 internal coordinates summarized in Figure 1. The values along the left y-axis can be thought of as percent contributions, since at all points along the IRC the sum of the y values for the curves is equal to 1.00. (Note, however, that individual y values may be slightly greater than one or slightly negative.) For example, at $s = -2.0$ in Figure 3a, the $1a_1$ normal mode is composed of roughly 80% β (*) and 20% γ (◇), with the remaining internal coordinates making essentially no contribution. Likewise, at $s = 1.8$, the $1a_1$ mode is composed of a 50:50 mixture of β and γ, with the remaining internals again making no contribution.

Figure 3a shows that the $1a_1$ mode is dominated throughout most of the reaction by the β motion. On the products side, the contribution of β decreases gradually with a concomitant increase in the contribution from γ. This is to be expected based on the fact that β and γ become equivalent at the product end point of the reaction. The perturbations around $s = -0.8$ and 0.0 may indicate subtle interactions with the reaction path. Since the dominant contribution to the $1a_1$ mode does not change (i.e., none of the curves cross), this indicates that the $1a_1$ mode is not involved in an avoided crossing with the other a_1 modes (with the possible

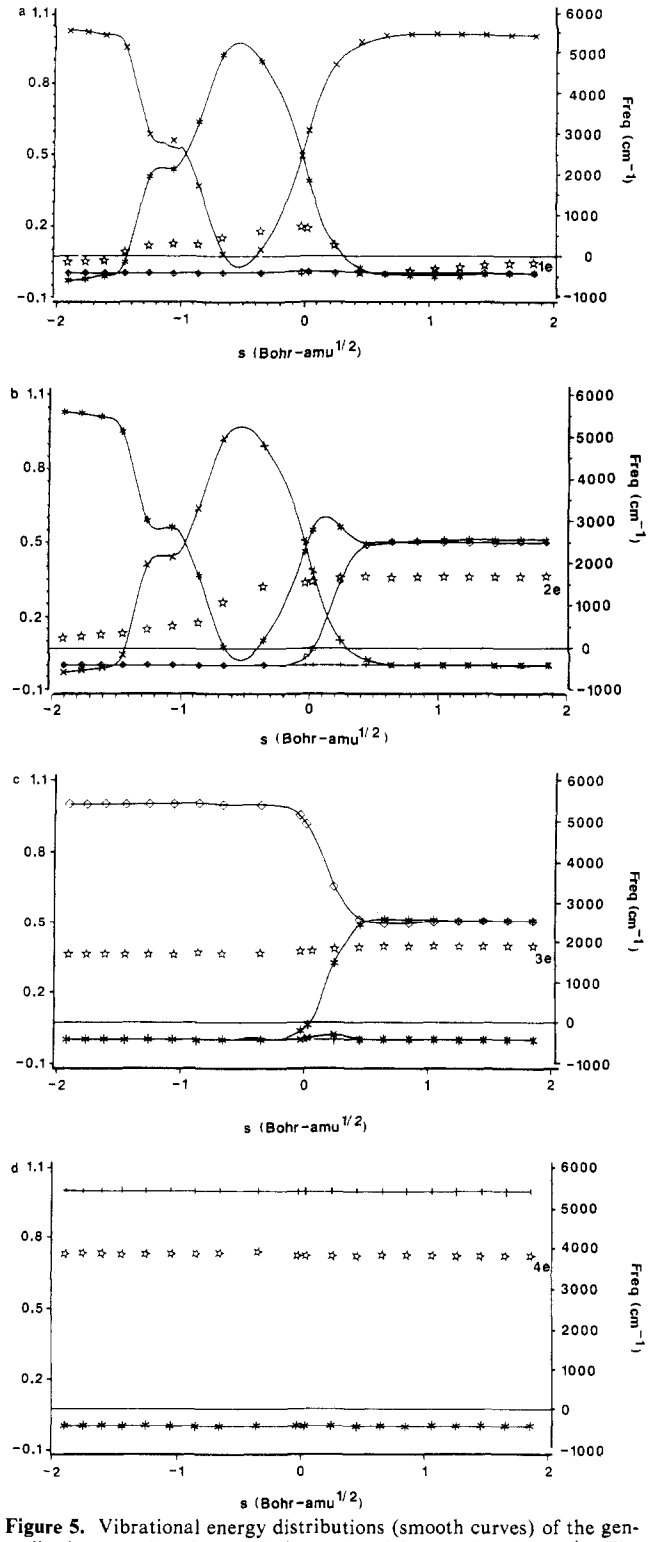

Figure 5. Vibrational energy distributions (smooth curves) of the generalized e normal modes and their associated frequencies (☆; cm^{-1}). The vertical axis on the left is unitless.

exception of the reaction path itself). Note that an avoided crossing with another a_1 mode would still be possible if that mode was also dominated by β; however, such is not the case in this reaction (vide infra).

Figure 3b is the analogous decomposition of the $2a_1$ normal mode. Here, we see three curve crossings at $s = -0.7$, 0.0, and +0.8. These locations correspond very closely to the three potential regions of avoided crossings in Figure 2. In the region from −2.0 to −0.7, the $2a_1$ mode is dominated by the intact C–H stretches of the methyl group (R_3, +). At about −0.7, the H–H stretch (r_1, Δ) curve rises to cross the R_3 curve and therefore becomes the primary contribution up to the transition state. Thus, this

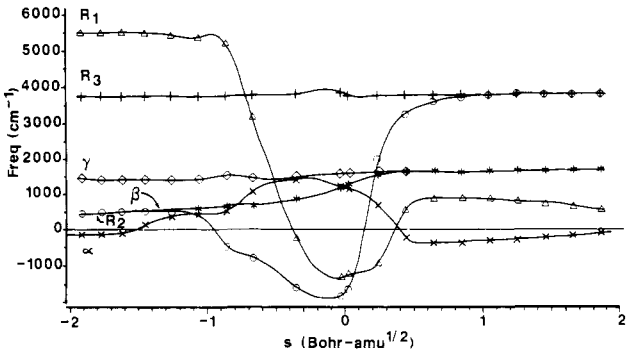

Figure 6. Intrinsic frequencies (cm^{-1}) along the $H_2 + CH_3 \rightarrow H + CH_4$ IRC.

is an avoided crossing of mode $2a_1$ with $3a_1$ along the IRC. At the transition state ($s = 0.0$), a second curve crossing (i.e., an avoided crossing with the reaction path) occurs, with the forming C–H bond (R_2, ⊙) becoming the dominant contributor. The final intersection takes place at $s = 0.8$, where R_3 reestablishes itself as the main contributor to $2a_1$. Note that this particular crossing does not actually correspond to a true avoided crossing of normal modes. The reason for this is that, in this region of the IRC, R_2 and R_3 are becoming equivalent internal coordinates and therefore should not be considered separately. Rather, the individual R_2 and R_3 curves should be summed and treated as a single coordinate.

Figure 3c is the analysis of vibrational mode $3a_1$. The interpretation here is similar to that in the preceding paragraph. The mode is initially dominated by contributions from R_1, the H–H stretch. At $s = -0.7$, R_3 takes over, illustrating the avoided crossing with $2a_1$. As in Figure 3b, the intersection of R_2 and R_3 at $s = 0.8$ is not indicative of an avoided crossing since these two internal coordinates are becoming equivalent in this region of the IRC.

It is important to qualitatively consider the nature of the reaction path. Clearly, the two most important processes in the reaction are the cleavage of the H–H bond and the formation of the C–H bond. Therefore, it is natural to expect that the reaction path can be described as a combination of these two internal parameters. One expects the forming C–H bond to be the primary component of the reaction path on the $H_2 + CH_3$ side of the reaction. Conversely, on the $H + CH_4$ side, one expects the breaking H–H bond to dominate the description of the reaction path. In the vicinity of the transition state, the reaction path is expected to be a roughly equal mixture of these two components. It is in this region that one expects avoided crossings between the reaction path and the transverse a_1 vibrations to facilitate the change from H–H character to C–H character. The reason, of course, that a quantitative characterization of the reaction path cannot be made is that it has been projected out of the calculated Hessians along the IRC.

The global picture one obtains for the evolution of the a_1 generalized normal modes is as follows. The $1a_1$ mode primarily describes the H–C–H angle bends and remains largely unchanged throughout the course of the reaction; i.e., it undergoes no avoided intersections with other a_1 vibrations. The $2a_1$ and $3a_1$ modes describe the intact C–H and H–H stretches, respectively, until they undergo an avoided crossing at $s = -0.8$. From this point on, mode $3a_1$ describes the intact C–H stretches. Mode $2a_1$, however, undergoes a second avoided intersection in the vicinity of the transition state (TS). This second crossing couples $2a_1$ and the reaction path. Thus, from the TS toward $H + CH_4$, the reaction path assumes the H–H character formerly found in the $2a_1$ mode. Likewise, the $2a_1$ mode takes on the former character of the reaction path, which is the stretch associated with the forming C–H bond (see the discussion of the reaction path in the previous paragraph). From the TS to products, no further avoided crossings occur. Returning to Figure 2, we see that the apparent avoided intersection between $1a_1$ and $2a_1$ near the TS actually does not involve mode $1a_1$ at all; rather, the crossing takes place between $2a_1$ and the reaction path. Furthermore, the possible avoided crossing at $s = 0.8$ does not occur at all. These interactions are reflected in the mode–mode couplings and reaction path curvature.[5]

We now proceed with a similar analysis of the e vibrations. Note that the complications associated with "hidden" couplings to the reaction path cannot occur here since the reaction path has a_1, rather than e, symmetry. Figure 4 shows the frequencies of generalized normal modes with e symmetry along the IRC. The 1e frequency actually becomes imaginary at $s = 0.3$, indicating the presence of a bifurcation[5,8] on the products side of the reaction path. The 1e frequency also is imaginary up to $s = -1.5$, but this may be due to numerical "noise" rather than an actual bifurcation on the reactants side. Both 1e and 2e frequencies approach zero on the reactants side, but only 1e goes to zero on the products side. There appears to be two possible avoided crossings, one potentially occurring between 1e and 2e around $s = -1.2$ and the other between 2e and 3e (and possibly involving 1e as well) around $s = 0.2$.

Figure 5a shows the composition of the 1e mode. Initially, 1e is largely composed of the degenerate linear H–H–C bend (α, ×). At $s = -1.0$, an avoided crossing between 1e and 2e occurs, which transforms 1e into the forming H–C–H bend (β, *). At the TS, 1e encounters another avoided crossing with 2e and returns to mainly α-character. Because 1e is the α-bend except in the region $-1.0 < s < 0.0$, it is necessary for this frequency to approach zero (see the ☆ curve) on both the reactants and products sides, since α becomes undefined as $s \rightarrow \pm\infty$.

Figure 5b illustrates the structure of the 2e mode. This mode starts out as primarily the forming H–C–H bend (β, *). As noted above, 2e undergoes an avoided crossing in the vicinity of $s = -1.0$, after which it is mainly described by α. At the TS, 2e encounters another crossing that reestablishes the β-character. After this point, 2e becomes an equal mixture of β and γ, which become equivalent internal coordinates on the product side of the reaction. As with the 1e frequency, the 2e frequency must approach zero on the reactants side. This is because the initial character of 2e is β, which becomes undefined as $s \rightarrow -\infty$.

Parts c and d of Figure 5 show the vibrational components of generalized normal modes 3e and 4e. Mode 3e (Figure 5c) is initially described as the intact H–C–H bends (γ, ◊) and evolves into an equal mixture of γ and β, which become symmetrically equivalent on the products side. Mode 4e (Figure 5d) describes the intact C–H stretches (R_3, +) throughout the entire course of the reaction.

The overall analysis of the evolution of the e modes is as follows. Modes 1e and 2e cross each other around $s = -1.0$ and cross a second time near the TS. Neither 3e or 4e undergoes any avoided intersections. While the first avoided intersection of modes 1e and 2e is expected on the basis of the projected frequencies in Figure 4, the second crossing near the TS is somewhat surprising, in spite of the sudden drop in frequency of the 1e mode.

Figure 6 is a plot of the intrinsic frequencies[7] of the 13 internal coordinates shown in Figure 1. The R_1 curve (△) is the H–H intrinsic frequency as a function of s. On the reactants side, the H–H bond has a large, positive intrinsic frequency. As one approaches the TS, however, the intrinsic frequency of H–H drops sharply and ultimately becomes imaginary (since the H–H stretch is intimately related to the reaction path). The H–H frequency becomes positive again as the reaction proceeds past the TS but approaches zero as the reaction is completed. The curve for the forming C–H bond (⊙) has just the opposite behavior. The forming C–H bond initially has an intrinsic frequency of zero and becomes slightly positive. As one comes closer to the TS, the C–H intrinsic frequency becomes imaginary, because, like the H–H bond, it is closely related to the reaction path. Beyond the TS, the forming C–H intrinsic frequency rises sharply and eventually merges with the intrinsic frequencies of the intact C–H bonds. The α-curve (×) starts at zero on the reactants side and gradually becomes positive as the TS is approached. Beyond the TS, the α-curve suddenly falls and becomes imaginary, suggesting that the bifurcation primarily involves the bending motion associated with this coordinate. As one proceeds to products, the α-curve

gradually rises to zero. Note that the initial and final values of zero for the α intrinsic frequency are consistent with the fact that α becomes undefined at both end points of the reaction. The β intrinsic frequency curve begins at zero and steadily rises until it merges with the γ-curve past the TS. This behavior is consistent with the fact that β is undefined at the reactants end point and is equivalent to γ at the products end point. As expected, the curves for the intact C-H stretches (R_3, +) and H-C-H bends (γ, ◊) show little change throughout the entire course of the reaction.

IV. Conclusions

The calculation of vibrational energy distributions and intrinsic frequencies along the $H_2 + CH_3 \rightarrow H + CH_4$ reaction path has been illustrated. These quantities provide a striking picture of the evolution of generalized normal coordinates and also reflect the changes in electronic structure during the course of a reaction. Furthermore, the energy distributions and intrinsic frequencies aid in the identification of couplings between individual generalized normal modes as well as between generalized modes and the reaction path.

Acknowledgment. This work was supported in part by grants from the National Science Foundation (CHE86-40771) and the Air Force Office of Scientific Research (87-0049). The computations were performed on the NDSU Quantum Chemistry Group VAX 8530 (provided with the aid of DOD Grant 86-0237), and the graphics were obtained with the aid of the NDSU IBM 3081-D32.

Registry No. H_2, 1333-74-0; CH_3, 2229-07-4.

Rate Constants for Reactions between Atmospheric Reservoir Species. 1. HCl

Ming-Taun Leu,* Shiro Hatakeyama,† and Kuang-Jung Hsu‡

Earth and Space Sciences Division, Jet Propulsion Laboratory, California Institute of Technology, Pasadena, California 91109 *(Received: November 28, 1988; In Final Form: February 28, 1989)*

The kinetics of the reactions of HCl with $ClONO_2$, N_2O_5, O_3, and HO_2NO_2 have been investigated by using a large-volume static reactor and a Fourier transform spectrometer (FTIR) at 296 K. The upper limits for the homogeneous gas-phase reaction rates of the $ClONO_2$ + HCl, N_2O_5 + HCl, O_3 + HCl, and HO_2NO_2 + HCl reactions were found to be 8.4×10^{-21}, 8.4×10^{-21}, 4.7×10^{-24}, and 9.0×10^{-22} (all in unit of $cm^3\ s^{-1}$), respectively. The heterogeneous nature of the $ClONO_2$ + HCl and N_2O_5 + HCl reactions are characterized in terms of the Langmuir-Rideal mechanism. The yields of HNO_3 were observed to be 0.94 ± 0.14 and 1.10 ± 0.12 for the $ClONO_2$ + HCl and N_2O_5 + HCl reactions, respectively, and the yield of $ClNO_2$ was found to be 0.84 ± 0.10 for the N_2O_5 + HCl reaction. The quoted errors represent one standard deviation of the measurement. In addition, an upper limit of 1.6×10^{-19} $cm^3\ s^{-1}$ at 296 K for the reaction of NO_3 with HCl was also obtained in this study. These results may be important in the elucidation of the role played by heterogeneous reactions in the development of the springtime Antarctic ozone depletion over the past decade.

Introduction

It is well-known that chemistry in the terrestrial atmosphere is governed by photolytic reactions and rapid free-radical reactions. Reactions between closed-shell molecules, such as the reaction of chlorine nitrate with hydrogen chloride, are usually ignored because their rates are generally expected to be much less than those with atomic or radical species. In the stratosphere there are several important closed-shell molecules that are temporary reservoir species of HO_x, NO_x, and ClO_x radicals. Concentrations of these reservoir species, in general, exceed those of atomic or radical species by several orders of magnitude. Consequently, slow gas-phase homogeneous reactions between them may be significant in stratospheric chemistry if these reactions can regenerate photochemically active molecules or produce more stable compounds. Heterogeneous counterparts of such reactions have also been suggested as potentially important in a recent review of atmospheric ozone.[1] For example, the $ClONO_2$ + HCl, $ClONO_2$ + H_2O, N_2O_5 + HCl, and N_2O_5 + H_2O reactions are frequently invoked to explain the significant depletion of springtime ozone in the Antarctic stratosphere[2-8] and also as a possible source of HNO_3 required in the winter at high latitudes in the stratosphere.[9]

In order to understand the kinetic nature of these reactions on various substrates, we have undertaken a systematic study of the following reactions involving HCl:

$$HCl + ClONO_2 \rightarrow Cl_2 + HNO_3 \quad (1)$$

$$HCl + N_2O_5 \rightarrow ClNO_2 + HNO_3 \quad (2)$$

$$HCl + O_3 \rightarrow HOCl + O_2 \quad (3)$$

$$HCl + HO_2NO_2 \rightarrow HOCl + HNO_3 \quad (4)$$

These reactions were carried out in a large-volume static reactor, and a Fourier transform infrared spectrometer was employed to provide the trace gas analysis.

Laboratory studies of reaction 1 using both static and flow systems have been reported recently. The first published study, which was performed by using a fast flow reactor coupled with a mass spectrometer as a detector, reported an upper limit for the homogeneous rate constant of 1.2×10^{-15} $cm^3\ s^{-1}$ at room temperature.[10] This value would suggest that the reaction of HCl

* To whom correspondence should be addressed.
† NRC/NASA Resident Research Associate (1985-1986). Permanent address: National Institute for Environmental Studies, P.O. Tsukuba-gakuen, Ibaraki 305, Japan.
‡ Permanent address: Department of Atmospheric Sciences, National Taiwan University, Taipei, Taiwan, R.O.C.

(1) Watson, R. T. *Atmospheric Ozone 1985*; World Meteorological Organization Global Ozone Research and Monitoring Project Report No. 16, Vol. 1, Chapter 2.
(2) Farman, J. C.; Gardiner, R. R.; Shanklin, J. D. *Nature* **1985**, *315*, 207.
(3) Solomon, S.; Garcia, R. R.; Rowland, F. S.; Wuebbles, D. J. *Nature* **1986**, *321*, 75.
(4) McElroy, M. B.; Salawitch, R. J.; Wofsy, S. C.; Logan, J. A. *Nature* **1986**, *321*, 759.
(5) Tung, K. K.; Ko, M. K. W.; Rodriguez, J. M.; Sze, N. D. *Nature* **1986**, *322*, 811.
(6) Crutzen, P. J.; Arnold, F. *Nature* **1986**, *324*, 651.
(7) Toon, O B.; Hamill, P.; Turco, R. P.; Pinto, J. *Geophys. Res. Lett.* **1986**, *13*, 1284.
(8) Rodriguez, J. M.; Ko, M. K. W.; Sze, N. D. *Geophys. Res. Lett.* **1986**, *13*, 1292.
(9) Austin, J.; Garcia, R. R.; Russell III, J. M.; Solomon, S.; Tuck, A. F. *J. Geophys. Res.* **1986**, *91*, 5477.

0022-3654/89/2093-5778$01.50/0